Land surface emissivity retrieval from multiple vegetation indices: a comparative study over India

T. Kodimalar, R. Vidhya & R. Eswar

Published online: 27 Nov 2019.

Submit your article to this journal ⬚

View related articles ⬚

View Crossmark data ⬚

Taylor & Francis
Taylor & Francis Group

Check for updates

Land surface emissivity retrieval from multiple vegetation indices: a comparative study over India

T. Kodimalar[a], R. Vidhya[a] and R. Eswar [b]

[a]Institute of Remote Sensing, Anna University, Chennai, India; [b]Department of Civil Engineering, Indian Institute of Technology Bombay, Mumbai, India

ABSTRACT

Land surface emissivity (LSE) is an important parameter used in the retrieval of land surface temperature (LST) from thermal infrared (TIR) sensors. One of the widely adopted methods for LSE estimation is to treat the LSE of a pixel as a linear combination of soil and vegetation emissivity and use Normalized Difference Vegetation Index (NDVI) for characterizing vegetation cover of the pixel. However, it is unclear if other existing vegetation indices (VI) can be used for estimating LSE using this method. The aim of this study is to compare multiple VIs: NDVI, Enhanced Vegetation Index (EVI), Normalized Difference Water Index (NDWI), Soil Adjusted Vegetation Index (SAVI) and Modified SAVI (MSAVI) for the retrieval of LSE over four sites in India with data from Landsat-7 and Landsat-8 satellites. The LSE estimated from different VIs were compared with the Advanced Spaceborne Thermal Emission Radiometer-Global Emissivity Dataset (ASTER GED) and MODIS 21 LST and emissivity product. It was found that EVI was marginally better performing than NDVI, consistently. However, EVI gave better results only under non- cropped conditions (NDVI < 0.25). Whereas, during cropped stages, NDWI performed better than other VIs for the retrieval of LSE. SAVI and MSAVI resulted in marginally poorer retrievals of LSE in comparison with other VIs and performed inconsistently.

1. Introduction

Land surface emissivity (LSE) is an intrinsic property of all the objects on earth and is dependent on the composition of the objects (Hulley et al. 2015). LSE is an important parameter required in the estimation of Land Surface Temperature (LST) observed from the thermal infrared (TIR) sensors aboard various remote sensing (RS) satellites. Since emissivity defines the efficiency with which an object can radiate energy, the knowledge of LSE is mandatory for not to overestimate the LST of surface objects. Mathematically, the problem of LST estimation is ill-posed as there is always N + 1 unknown for N equations where N is the number of TIR channels in a sensor. The N + 1 unknown correspond to LSE in each of the N channels and the LST itself (Li, Tang, and Wu et al. 2013). For sensors with multiple TIR channels such as the Advanced Spaceborne Thermal Emission and reflection Radiometer (ASTER), LSE and LST are retrieved together from TIR radiance data itself after forcing some assumptions and constraints on the radiative transfer equation (RTE) (Li et al. 2012). However, for sensors with single thermal band such as the Landsat-7 Enhanced Thematic

CONTACT T. Kodimalar ✉ tkodimalar@gmail.com 🌐 Institute of Remote Sensing, Anna University, Chennai, 600025, India

Mapper+ (ETM+), it becomes necessary to estimate LSE separately for further use in the determination of LST. Even in the case of Landsat-8 Thermal Infrared Sensor (TIRS) with two thermal channels, the stray light issue had affected the calibration of the sensor and it is recommended to use only the band 10 for LST retrieval (USGS 2019). Under these circumstances, where LSE has to be estimated separately, either a land cover classification-based approach (e.g., Snyder et al. 1998) or Normalized Difference Vegetation Index (NDVI) based approach (e.g., Valor and Caselles 1996) is traditionally used (Li et al. 2012). The NDVI-based methods were developed on the premise that a land surface pixel is a mixture of vegetation and soil and the effective pixel emissivity can be estimated as the linear combination of the individual component emissivity (Sobrino and Raissouni 2000). The simplicity and accuracy of this NDVI-based method led to its widespread usage across the globe (Sobrino et al. 2008; Cristobal et al., 2009; Srivastava, Majumdar, and Bhattacharya 2009; Jiménez-Muñoz, Cristóbal, and Sobrino et al. 2009). It is to be noted that in the above-mentioned method, only NDVI was used as an indicator of vegetation for estimating the fraction vegetation cover (FVC) of a pixel. Apart from NDVI, there are several other vegetation indices (VI) such as the Normalized Difference Water Index (NDWI, Gao 1996), Enhanced Vegetation Index (EVI, Huete and Justice 1999), Soil-Adjusted Vegetation Index (SAVI, Huete 1988) etc., that characterizes different properties of the vegetation. However, the applicability of these multiple VIs for the estimation of LSE is yet to be tested. Though Mallick et al. (2012) used NDWI for the estimation of LSE, a comparative analysis on the accuracy of the LSE retrieval using multiple VIs was not performed. Hence, the aim of this study is to compare the applicability of five different VIs such as NDVI, EVI, NDWI, SAVI and Modified SAVI (MSAVI, Qi et al. 1994) for the estimation of LSE. The objective is developed based on the premises of an earlier study (Eswar, Sekhar, and Bhattacharya 2016) which compared the role of different VIs on spatial disaggregation of LST data. The study found out that NDVI performed better only for wet conditions and NDWI performed better for LST disaggregation during drier conditions. A similar analogy can be arrived for LSE also and it is the aim of this study to test whether such a difference in performance is observed among the multiple VIs.

These five indices were selected as they indicate different properties of vegetation: NDVI represents vegetation vigour (Gu et al. 2007), EVI is found to be highly correlated with Leaf Area Index, and further is less sensitive to saturation, soil and atmospheric effects (Jiang et al. 2008), NDWI is an indicator of vegetation liquid water content (Gao 1996) and SAVI and MSAVI were developed to minimize the soil effects while observing vegetation (Huete 1988; Qi et al. 1994). In addition to these properties, these five indices are provided as a part of Landsat vegetation indices product (USGS 2017) and hence is commonly and easily available to the remote sensing community at a high spatial resolution. A different definition of NDWI and a modified NDWI (MNDWI) (McFeeters 1996; Xu 2006) that are related to open waterbodies are also in use. However, in this study, we have used the NDWI as defined by Gao (1996) that is related to vegetation liquid water content. Some literature refers to the NDWI by Gao (1996) as Normalized Difference Moisture Index (NDMI). However, we have retained the original name given by Gao (1996) in this study.

2. Study area and datasets

2.1. Study area

Four spatial grids in India each of size 96 km × 96 km were chosen in the states of Punjab (Grid 1), Madhya Pradesh (Grid 2), Gujarat (Grid 3) and Karnataka (Grid 4) for the study. Grid 1, located in the Punjab state in the North of India, is one of the intensively cultivated areas due

to its location on fertile alluvial deposits. The region is semi-arid with an annual rainfall of 600–800 mm. Grid 2 is in the state of Madhya Pradesh (Central India) and has an annual rainfall in the range of 800–1200 mm. Further, the air temperature in the spatial grid varies between 42°C in May to about 11°C in January. The area predominantly has black soils with sandy to clay loam texture. Grid 3 is located in the Western part of India in the state of Gujarat with an annual rainfall of around 900–1100 mm with a major share of rainfall during the summer monsoon season (June–September) and the temperature varying between 12°C and 40°C. The area is primarily dominated by sandy loam-textured soil and the winter cropping in not done as intensively as grids 1 or two. Grid 4 is located in the Peninsular India and has a complex mix of landscape such as croplands, forests, mountain ranges and settlements. The grid exhibits a steep gradient in rainfall varying from 500 mm year^{-1} in the northeastern parts to 1200 mm year^{-1} in the southwestern parts (Eswar, Sekhar, and Bhattacharya 2016). The grid also has a mixed agriculture practice with varieties of crops such as sugarcane, pulses, vegetables being cultivated. The grids were chosen such that they represent different climatic conditions and agricultural practices. Additional information about the spatial grids is provided in Table 1 and the location of the grids is shown in Figure 1.

2.2. Satellite data

For this study, a total of 17 Landsat-7 ETM+ and 5 Landsat-8 Operational Land Imager (OLI) collection 1, level 2 images containing the atmospherically corrected surface reflectance data were used (Masek et al. 2006). Among the 17 Landsat-7 images, 6 were over grid 1, three were over grid 2, 5 were over grid 3 and 3 were over grid 4. The five Landsat-8 images were acquired over grid 4 (denoted as KL81–KL85 in Table 2). The images were acquired such that they capture different crop covers in the two major cropping seasons in India (Kharif, summer monsoon cropping season and Rabi, winter cropping season). Information about the images, time of acquisition, etc., are provided in Table 2.

In addition to Landsat images, ASTER Global Emissivity Dataset (ASTER GED, Hulley et al. 2015) and MODIS 21 land surface temperature and emissivity (LST&E) product were used as reference. The version 3.0 of the ASTER GED which represents the average emissivity value during the period 2000–2008 at a spatial resolution of 100 m was selected for comparison with the Landsat-7 derived emissivity. Though the GED product is constant over time and may not account for vegetation phenology (Malakar et al. 2018), this is the only reliable high spatial resolution emissivity dataset available for the globe and has been used in several studies as reported by Hulley et al. (2015). Since ASTER GED version 3.0 is not available after 2008, MODIS 21 LST&E product at 1000 m resolution was used as a reference for comparing the LSE derived from Landsat-8 images. The LSE from both the products was developed using the Temperature Emissivity Separation (TES) algorithm with a water vapour scaling correction method (Hulley,

Table 1. Details about the four spatial grids.

| Grid	Location	Geographical extent	Climate (Peel, Finlayson, and McMahon 2007)	Major vegetation/crops
Grid 1	Punjab	29.95⁰ N – 30.82⁰ N 74.97⁰ E – 75.97⁰ E	Arid steppe	Rice and wheat
Grid 2	Madhya Pradesh	22.39⁰ N – 23.27⁰ N 77.17⁰ E – 78.12⁰ E	Tropical Savannah	Soya bean, wheat and chick pea
Grid 3	Gujarat	22.63⁰ N – 23.51⁰ N 72.76⁰ E – 73.71⁰ E	Arid Steppe/Tropical Savannah	Cotton, Rice, wheat and tobacco
Grid 4	Karnataka	11.44⁰ N – 12.31⁰ N 76.25⁰ E – 77.14⁰ E	Tropical Monsoon/Savannah	Rice, Sugarcane, pulses, vegetables
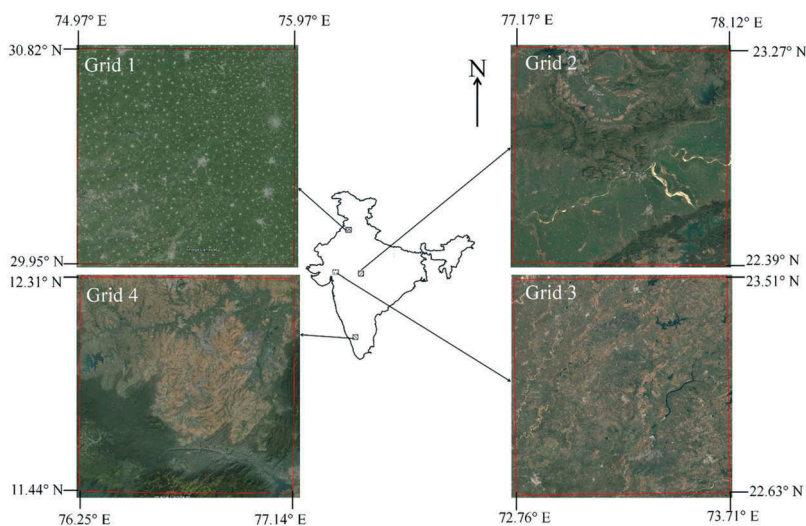
Figure 1. Spatial grids selected for the study.

Table 2. Information about the satellite data.

Spatial grid	Notation used in the paper	Date of acquisition	Path	Row	Mean NDVI
Grid 1	P1	9 December 2000	148	39	0.36
	P2	25 December 2000			0.50
	P3	2 May 2001			0.14
	P4	10 November 2001			0.17
	P5	21 May 2002			0.13
	P6	8 May 2003			0.14
Grid 2	M1	21 January 2001	145	44	0.44
	M2	26 March 2001			0.19
	M3	21 September 2002			0.59
Grid 3	G1	20 September 2000	148	44	0.50
	G2	22 October 2000			0.40
	G3	23 November 2000			0.30
	G4	10 January 2001			0.32
	G5	11 February 2001			0.30
Grid 4	K1	14 January 2001	144	52	0.48
	K2	3 March 2001			0.38
	K3	3 December 2002			0.56
	KL81	18 January 2017			0.41
	KL82	3 February 2017			0.40
	KL83	6 February 2018			0.45
	KL84	22 February 2018			0.43
	KL85	14 April 2019			0.35

Malakar, and Freepartner 2016). The MODIS 21 product is generated operationally and hence can capture vegetation phenology. The 8-day composite LST&E images coincident with the acquisition dates of Landsat-8 were downloaded and used here.

3. Methodology

3.1. Model description

The LSE model used in this study is based on the model proposed by Sobrino and Raissouni (2000) and the model estimates the LSE of a mixed pixel as a linear combination of the emissivities of vegetation (ε_v, considered as 0.985) and soil (ε_s)

$$\varepsilon = f_v \varepsilon_v + (1 - f_v)\varepsilon_s + c \tag{1}$$

where ε is the LSE of a pixel, f_v is the fraction of vegetation in the pixel and c is the cavity term that accounts for the radiance reaching the sensor due to the internal reflections from the roughness elements in the pixel (Valor and Caselles 1996). In the above equation, ε_s was estimated as a linear function of surface reflectance in the red band (as explained below) and f_v was estimated as (Sobrino and Raissouni 2000):

$$f_v = \left(\frac{VI - VI_s}{VI_v - VI_s}\right)^2 \tag{2}$$

where VI is the selected vegetation index and the subscripts s and v indicate the VI values for pure soil and pure vegetation pixels, respectively. Traditionally, only NDVI is used in Equation (2) for the estimation of f_v whereas, in this study, five different VIs as given in Section 1 will be used with each index having their own soil and vegetation limits (explained below). Further, if the f_v value of any pixel was either found to be negative or greater than one, they were replaced with zero and one, respectively. The cavity term in Equation (1) was calculated as given in Equation (3) (Srivastava, Majumdar, and Bhattacharya 2009).

$$c = 4 < d\varepsilon > f_v(1 - f_v) \tag{3}$$

In Equation (3), $< d\varepsilon >$ represents the mean value of the cavity effect which is assumed to be 0.005 (Srivastava, Majumdar, and Bhattacharya 2009) in this work. However, for pixels classified as pure vegetation pixels ($f_v = 1$), the cavity term in Equation (1) was assumed to be 0.005 without computing it from Equation (3).

Two important parameters of the LSE model explained here are the thresholds of various VIs corresponding to soil and vegetation and the soil emissivity. The NDVI values corresponding to soil and vegetation were approximated to be 0.2 and 0.6, respectively, based on the analysis of multi-temporal satellite images for the spatial grids combined with knowledge from the literature. However, the soil and vegetation thresholds for other VIs such as the EVI, NDWI, SAVI and MSAVI have to be established for the study grids. For doing this, the mean VI (all the five VIs) values for all the satellite images were computed and a linear regression was performed between the mean NDVI values and other four VIs. This resulted in four regression equations relating NDVI with other four indices (viz. EVI, NDWI, SAVI and MSAVI). Then, in the four regression equations, the soil and vegetation NDVI values (0.2 and 0.6, respectively) were substituted to estimate the soil and vegetation thresholds of other VIs. The threshold values are tabulated in Table 3. Similarly, the other important value in the model is the emissivity of soil which was estimated from the relationship between soil reflectance in red band and soil emissivity (Sobrino et al. 2008). The reflectance spectra for the major classes of soils in the study area were identified from the ASTER Spectral library (total of 15 soils). Then, for each soil type, the reflectance spectra corresponding to the red band of the ETM+ and OLI sensors were extracted and similarly, for the TIR band (corresponding to band 6 in Landsat-7 and band 10 in Landsat-8), the reflectance spectra were converted into emissivity spectra (emissivity = 1 − reflectance). The multiple reflectances and emissivity values extracted from ASTER spectral library were then averaged to get the mean reflectance in the red band (ρ_{red}) and mean emissivity in the TIR band for each soil type. Finally, a regression was performed between the red reflectance and TIR emissivity of all the soil types in the spatial grids to yield the following equations. Here, Equation (4) is for estimating the soil emissivity ($\varepsilon_{s,Landsat-7}$) corresponding to

band 6 of Landsat-7, and similarly, Equation (5) is for estimating the soil emissivity ($\varepsilon_{s,Landsat-8}$) corresponding to band 10 of Landsat-8.

$$\varepsilon_{s,Landsat-7} = -0.0408\rho_{red} + 0.9796 \tag{4}$$

$$\varepsilon_{s,Landsat-8} = -0.0475\rho_{red} + 0.9788 \tag{5}$$

The equations given above are used along with Equation (1–3) for estimating the emissivity at the pixel scale.

3.2. Satellite data processing

The surface reflectance data from the ETM+ and OLI sensors were first extracted for the study area and resampled to 50 m from the original 30 m resolution. Then, the multiple vegetation indices were computed based on the equations given in Tables 4 and 5 (USGS 2017) and the computed VIs were spatially averaged to 100 m and 1000 m spatial resolution for ETM+ and OLI data, respectively, to match with the spatial resolution of ASTER GED and MODIS 21 products. The multiple VIs were then used in the LSE model for the retrieval of land emissivity.

Similarly, the ASTER GED data were also extracted and cropped to the study area. The GED data have emissivity values corresponding to the five spectral bands of the ASTER sensor. This multi-band spectral emissivity was converted into Landsat-7 spectral emissivity using the equation (Malakar et al. 2018):

$$\varepsilon_{L7} = 0.2147\varepsilon_{A13} + 0.7789\varepsilon_{A14} + 0.0058 \tag{6}$$

In the above equation, ε_{L7} denote Landsat-7 spectral emissivity and ε_{A13} and ε_{A14} denote the spectral emissivities in bands 13 and 14 of the ASTER sensor. This LSE was used as the reference to compare the LSE retrieved from Landsat-7 at 100 m spatial resolution. The LSE derived from Landsat-8 was directly compared with the emissivity of band 31 from the MODIS 21 LST&E product available at 1000 m spatial resolution.

The LSE estimated from Landsat using the five VIs were compared against the reference emissivity datasets for identifying the better performing index. The result of a comparison is expressed as Root Mean Square Error (RMSE) given by

$$\text{RMSE} = \left[n^{-1} \sum_{i=1}^{n} \left(\varepsilon_{modelled}[i] - \varepsilon_{reference}[i] \right)^2 \right]^{\frac{1}{2}} \tag{7}$$

Here, $\varepsilon_{modelled}$ is the LSE estimated from Landsat and $\varepsilon_{reference}$ represents the reference emissivity data (ASTER GED for Landsat-7 and MODIS 21 product for Landsat-8), i is each pixel in the image, n is the total number of pixels in an image.

Table 3. Soil and vegetation thresholds for the five VIs.

Vegetation index	Soil threshold	Vegetation threshold
NDVI	0.20	0.60
EVI	0.12	0.41
NDWI	−0.02	0.40
SAVI	0.12	0.38
MSAVI	0.10	0.37

Table 4. Equations for the five VIs used in this study.

VI	Equation[a]
NDVI	$\dfrac{\rho_{NIR}-\rho_{red}}{\rho_{NIR}+\rho_{red}}$
EVI	$\dfrac{2.5(\rho_{NIR}-\rho_{red})}{\rho_{NIR}+6\rho_{red}-7.5\rho_{blue}+1}$
NDWI	$\dfrac{\rho_{NIR}-\rho_{SWIR}}{\rho_{NIR}+\rho_{SWIR}}$
SAVI	$\dfrac{\rho_{NIR}-\rho_{red}}{\rho_{NIR}+\rho_{red}+0.5}(1+0.5)$
MSAVI	$\dfrac{(2\rho_{NIR})+1-\sqrt{(2\rho_{NIR}+1)^{2}-8(\rho_{NIR}-\rho_{red})}}{2}$

[a]ρ_{band} refers to the surface reflectance value in the corresponding band. NIR: near-infrared band, red: red band, SWIR: shortwave infrared band and blue: blue band.

Table 5. Band numbers in Landsat-7 and Landsat-8 satellites corresponding to different portions of the electromagnetic spectrum mentioned in Table 4.

Satellite	Blue	Red	Near infrared	Shortwave infrared
Landsat-7	1	3	4	5
Landsat-8	2	4	5	6

4. Results and discussions

The results are first presented for the LSE modelled using Landsat-7 and then using Landsat-8. The mean NDVI of all the Landsat-7 satellite scenes analysed are presented in Table 2. For the purpose of discussions, we have classified the scenes with mean NDVI greater than or equal to 0.25 as vegetated and those having less than 0.25 as non-vegetated scenes. Based on this threshold, there were 12 vegetated (P1, P2, M1, M3, G1–G5, K1–K3) and 5 non-vegetated (P3–P6, M2) scenes.

The LSE estimated from Landsat-7 was compared with ASTER GED for finding the best performing VI. For the vegetated scenes, the RMSE of the retrieved LSE were in the range of 0.010–0.016, 0.008–0.014, 0.009–0.016, 0.010–0.017, 0.010–0.017 for NDVI, NDWI, EVI, SAVI and MSAVI-based retrievals, respectively, and similarly, for the non-vegetated scenes, the RMSE were in the range of 0.004–0.005, 0.004–0.006, 0.003–0.005, 0.003–0.005, 0.003–0.005 for the five indices in the same order. The RMSE of individual scenes are tabulated in Table 6. From the RMSE values, it can be observed that the errors in the retrieved LSE were higher for vegetated scenes than non-vegetated scenes. This may be because of the fact that ASTER GED is a time-averaged LSE product without considering the effect of vegetation phenology (Malakar et al. 2018). It was further observed that the RMSE of the LSE retrieved using EVI was marginally smaller than the LSE retrieved using NDVI. In addition, EVI-based retrieval performed better than SAVI and MSAVI also for almost all the analysed satellite scenes. There was a difference in performance observed between the LSE estimated from EVI and NDWI. For vegetated scenes, LSE estimated based on NDWI provided relatively lower RMSE than EVI-based estimation. However, for non-vegetated scenes, EVI performed better in retrieving LSE than NDWI for all the satellite scenes.

The results obtained are further tested by comparing the VI derived emissivity from Landsat-8 and MOD21 emissivity (Table 7). Since SAVI and MSAVI performed marginally poorer that EVI and NDWI for non-vegetated and vegetated cases, respectively, they were excluded from this analysis. The results from Landsat-8 further confirm the results obtained

Table 6. RMSE values for the LSE estimated from Landsat-7 images.

| Grid	Case	Vegetated/non-vegetated	Mean NDVI	Root-mean-square error				
				NDVI	EVI	NDWI	SAVI	MSAVI
Grid 1	P1	Vegetated	0.36	0.0102	0.0094	0.0083	0.0095	0.0095
	P2	Vegetated	0.50	0.0125	0.0125	0.0122	0.0125	0.0125
	P3	Non-vegetated	0.14	0.0037	0.0034	0.0042	0.0035	0.0035
	P4	Non-vegetated	0.17	0.0053	0.0051	0.0062	0.0052	0.0052
	P5	Non-vegetated	0.13	0.0044	0.0041	0.0050	0.0042	0.0042
	P6	Non-vegetated	0.14	0.0043	0.0042	0.0051	0.0043	0.0043
Grid 2	M1	Vegetated	0.44	0.0105	0.0100	0.0096	0.0100	0.0100
	M2	Non-vegetated	0.19	0.0051	0.0050	0.0065	0.0051	0.0051
	M3	Vegetated	0.59	0.0131	0.0129	0.0111	0.0130	0.0130
Grid 3	G1	Vegetated	0.50	0.0164	0.0163	0.0117	0.0166	0.0166
	G2	Vegetated	0.40	0.0135	0.0133	0.0096	0.0141	0.0141
	G3	Vegetated	0.30	0.0101	0.0101	0.0091	0.0103	0.0103
	G4	Vegetated	0.32	0.0109	0.0109	0.0104	0.0110	0.0110
	G5	Vegetated	0.30	0.0102	0.0103	0.0100	0.0104	0.0104
Grid 4	K1	Vegetated	0.48	0.0151	0.0148	0.0132	0.0151	0.0151
	K2	Vegetated	0.38	0.0136	0.0128	0.0126	0.0132	0.0132
	K3	Vegetated	0.56	0.0165	0.0164	0.0142	0.0167	0.0167

Table 7. RMSE values for the LSE estimated using multiple VI from Landsat-8 images.

Grid	Case	Vegetated/non-vegetated	Mean NDVI	Root-mean-square error		
				NDVI	EVI	NDWI
Grid 4	KL81	Vegetated	0.41	0.0076	0.0066	0.0060
	KL82	Vegetated	0.40	0.0060	0.0049	0.0046
	KL83	Vegetated	0.45	0.0063	0.0054	0.0046
	KL84	Vegetated	0.43	0.0063	0.0054	0.0048
	KL85	Vegetated	0.35	0.0130	0.0122	0.0103

from the Landsat-7 data. For additional analysis, differenced RMSE ($RMSE_{EVI}$-$RMSE_{NDWI}$) was plotted against the mean NDVI of the scene for the 17 Landsat-7 images and the plot is presented in Figure 2. It can clearly be observed from Figure 2 that for non-vegetated conditions the $RMSE_{NDWI}$ was relatively higher than $RMSE_{EVI}$ resulting in negative differences. For vegetated scenes, $RMSE_{EVI}$ was higher than $RMSE_{NDWI}$. A regression relationship was developed between the differenced RMSE and the mean NDVI which further indicated that there is an increase in the differenced RMSE with an increase in NDVI. The regression line intercepted the zero-differenced RMSE (ordinate) value around the NDVI value of 0.25. In summary, the results demonstrated that EVI is better suited for LSE estimation for non-vegetated conditions, whereas NDWI is more suited for vegetated conditions.

5. Conclusions

LSE is a property of the land surface and is a critical input in the estimation of LST. LSE is primarily estimated from NDVI when no other source of LSE is available. This study compared five different VIs: NDVI, EVI, NDWI, SAVI and MSAVI for the estimation of LSE using a simple model proposed by Sobrino and Raissouni (2000). Data from Landsat-7 ETM+ and Landsat-8 OLI sensors were used in the study and the estimated LSE was compared against the ASTER Global Emissivity Dataset and LSE from MODIS 21 land surface temperature and emissivity product. It was observed that EVI performed marginally better than NDVI for all the analysed
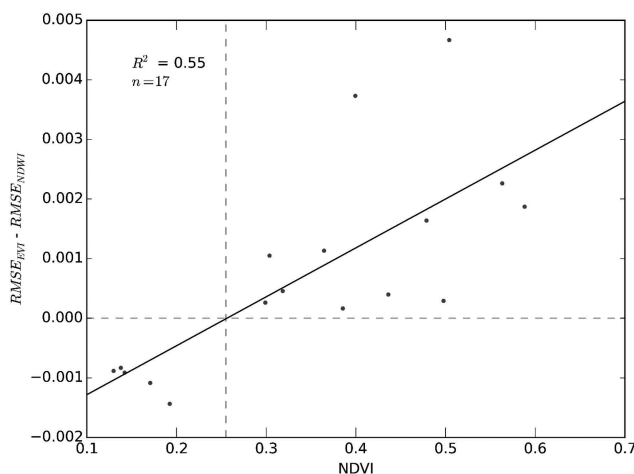
Figure 2. Scatter plot of the difference between RMSE$_{EVI}$ and RMSE$_{NDWI}$ versus mean NDVI.

satellite scenes. Hence, LSE from EVI was then compared with other VIs. It was found out that for non-vegetated satellite scenes, LSE retrieved using EVI was having lower RMSE than LSE retrieved using other VIs. However, for vegetated scenes, NDWI was the better performing index for the estimation of LSE. Hence, a proper choice should be made in choosing the vegetation index for the estimation of LSE using vegetation index-based methods. This result will be of importance especially in the retrieval of LST using algorithms that require LSE to be independently estimated and passed as input to the LST retrieval algorithm. Future studies will be directed towards further testing the results of this study using *in-situ* data.

ORCID

R. Eswar 🆔 http://orcid.org/0000-0001-6227-4873

References

Cristobal, J., J. C. Jimnez-Munoz, J. A. Sobrino, M. Ninyerola, and X. Pons. 2009. "Improvements in Land Surface Temperature Retrieval from the Landsat Series Band Using Water Vapour and Air Temperature." *Journal of Geophysical Research* 114: D08103. doi:10.1029/2008JD010616.

Eswar, R., M. Sekhar, and B. K. Bhattacharya. 2016. "Disaggregation of LST over India: Comparative Analysis of Different Vegetation Indices." *International Journal of Remote Sensing* 37 (5): 1035–1054. doi:10.1080/01431161.2016.1145363.

Gao, B.-C. 1996. "NDWI-A Normalized Difference Water Index for Remote Sensing Vegetation Liquid Water from Space." *Remote Sensing of Environment* 58: 257–266. doi:10.1016/S0034-4257(96)00067-3.

Gu, Y., J. F. Brown, J. P. Verdin, and B. Wardlow. 2007. "A Five-year Analysis of MODIS NDVI and NDWI for Grassland Drought Assessment over the Central Great Plains of the United States." *Geophysical Research Letters* 34: L06407. doi:10.1029/2006GL029127.

Huete, A., and Justice, C. (1999). "MODIS Vegetation Index, Algorithm Theoretical Basis Document", Accessed from: https://modis.gsfc.nasa.gov/data/atbd/atbd_mod13.pdf, last accessed on 17-Nov-2019

Huete, A. R. 1988. "A Soil-Adjusted Vegetation Index (SAVI)." *Remote Sensing of Environment* 25: 295–309. doi:10.1016/0034-4257(88)90106-X.

Hulley, G., N. Malakar, and R. Freepartner. 2016. "MODIS Land Surface Temperature and Emissivity Product (Mxd21) Algorithm Theoretical Basis Document." Jet Propulsion Laboratory Publication. 12–17. Accessed 15 September 2019. https://modis.gsfc.nasa.gov/data/atbd/atbd_mod21.pdf

Hulley, G. C., S. J. Hook, E. Abbott, N. Malakar, T. Islam, and M. Abrams. (2015). "The ASTER Global Emissivity Dataset (ASTER GED): Mapping Earth's emissivity at 100 meter spatial scale", *Geophysical Research Letters*, 42, 7966–7976. doi:10.1002/2015GL065564

Jiang, Z., A. R. Huete, K. Didan, and T. Miura. 2008. "Development of a Two-Band Enhanced Vegetation Index without a Blue Band." *Remote Sensing of Environment* 112: 3833–3845. doi:10.1016/j.rse.2008.06.006.

Jiménez-Muñoz, J. C., J. Cristóbal, J. A. Sobrino, G. Soria, M. Ninyeroal, and X. Pons. 2009. "Revision Of The Single-channel Algorithm for Land Surface Temperature Retrieval from Landsat Thermal-infrared Data." *Ieee Transactions on Geoscience and Remote Sensing* 47 (1): 339-349. doi: 10.1109/TGRS.2008.2007125.

Li, Z. L., Tang, B.H., Wu, H., Ren, H., Yan, G., Wan, Z., Trigo, I.F. and Sobrino, J.A., 2013. "Satellite-derived land surface temperature: Current status and perspectives." *Remote Sensing of Environment*, 131 :14–37. doi: 10.1016/j.rse.2012.12.008.

Li, Z. L., H. Wu, N. Wang, S. Qiu, J. A. Sobrino, Z. Wan, B.-H. Tang, et al. 2012. "Land Surface Emissivity Retrieval from Satellite Data." *International Journal of Remote Sensing* 34 (9–10): 3084–3127. doi:10.1080/01431161.2012.716540.

Malakar, N. K., Hulley, G.C., Hook, S.J., Laraby, K., Cook, M. and Schott, J. R.. 2018. "An Operational Land Surface Temperature Product for Landsat Thermal Data: Methodology and Validation." *IEEE Transactions on Geoscience and Remote Sensing*, 56(10): 5717–5735. doi: 10.1109/TGRS.2018.2824828.

Mallick, J., C. K. Singh, S. Shashtri, A. Rahman, and S. Mukherjee. 2012. "Land Surface Emissivity Retrieval Based on Moisture Index from Landsat TM Satellite Data over Heterogeneous Surfaces of Delhi City." *International Journal of Applied Earth Observation and Geoinformation* 19: 348–358. doi:10.1016/j.jag.2012.06.002.

Masek, J.G., Vermote, E.F., Saleous, N., Wolfe, R., Hall, F.G., Huemmrich, F., Gao, F., Kutler, J., and Lim, T.K. 2006. "A Landsat surface reflectance data set for North America, 1990-2000." *IEEE Geoscience and Remote Sensing Letters* 3, 68-72.

McFeeters, S. K. 1996. "The Use of Normalized Difference Water Index (NDWI) in the Delineation of Open Water Features." *International Journal of Remote Sensing* 17: 1425–1432. doi:10.1080/01431169608948714.

Peel, M. C., B. L. Finlayson, and T. A. McMahon. 2007. "Updated World Map of the Köppen-Geiger Climate Classification." *Hydrology and Earth System Sciences* 11: 1633–1644. doi:10.5194/hess-11-1633-2007.

Qi, J., A. Chehbouni, A. R. Huete, Y. H. Kerr, and S. Sorooshian. 1994. "A Modified Soil Adjusted Vegetation Index." *Remote Sensing of Environment* 48: 119–126. doi:10.1016/0034-4257(94)90134-1.

Snyder, W. C., Z. Wan, Y. Zhang, and Y. Z. Feng. 1998. "Classification-Based Emissivity for Land Surface Temperature Measurement from Space." *International Journal of Remote Sensing* 19: 2753–2774. doi:10.1080/014311698214497.

Sobrino, J. A., J. C. Jimenez-Munoz, G. Soria, M. Romaguera, L. Guanter, J. Moreno, A. Plaza, and P. Martincz. 2008. "Land Surface Emissivity Retrieval from Different VNIR and TIR Sensors." *IEEE Transactions on Geoscience and Remote Sensing* 46: 316–327. doi:10.1109/TGRS.2007.904834.

Sobrino, J. A., and Raissouni, N. 2000. "Toward Remote Sensing Methods for Land Cover Dynamic Monitoring: Application to Morocco." *International Journal of Remote Sensing*, 21: 353–366. doi: 10.1080/014311600210876.

Srivastava, P. K., T. J. Majumdar, and A. K. Bhattacharya. 2009. "Surface Temperature Estimation in Singhbhum Shear Zone of India Using Landsat-7 ETM+ Thermal Infrared Data." *Advances in Space Research* 43: 1563–1574. doi:10.1016/j.asr.2009.01.023.

USGS. 2017. "Landsat Surface Reflectance Derived Spectral Indices, Product Guide, Version 3.6." Accessed 14 September 2019. https://landsat.usgs.gov/sites/default/files/documents/si_product_guide.pdf

USGS. 2019. "Landsat 8 Data Users Handbook, Version 4.0." Accessed 14 September 2019. https://prd-wret.s3-us-west-2.amazonaws.com/assets/palladium/production/atoms/files/LSDS-1574_L8_Data_Users_Handbook_v4.pdf

Valor, E., and V. Caselles. 1996. "Mapping Land Surface Emissivity from NDVI: Application to European, African, and South American areas." *Remote Sensing of Environment* 57: 167–184. doi:10.1016/0034-4257(96)00039-9.

Xu, H. 2006. "Modification of Normalized Difference Water Index (NDWI) to Enhance Open Water Features in Remotely Sensed Imagery." *International Journal of Remote Sensing* 27 (14): 3025–3033. doi:10.1080/01431160600589179.